Water Practice & Technology Vol 15 No 3
doi: 10.2166/wpt.2020.056

Thermodynamics, kinetics, and isotherms for phenol removal from wastewater using red mud

Ashanendu Mandal[a], Basab Brata Dey[a,b] and Sudip Kumar Das[a,*]

[a] Chemical Engineering Department, University of Calcutta, 92, APC Road, Kolkata 700009, India

[b] Biochemistry Department, University of Calcutta, 35, Ballygunge Circular Road, Ballygunge, Kolkata 700019, India

*Corresponding author. E-mail: drsudipkdas@gmail.com

Abstract

The phenol removal through adsorption using industrial waste has been studied. The red mud generated as waste in the aluminum plants was used in this research. The surface characterizations of red mud were assessed. The batch experiment was investigated with pH (2–12), adsorption period (120–600 min), phenol content (40–200 mg/L), adsorbent dose (2–7 g/L), and temperature (30–50 °C). At the optimum operating condition, the percentage of phenol removal was 87.5%. The pseudo-second-order kinetic model ($r^2 = 0.98625$–0.99994) fitted better than the pseudo-first-order kinetic model. The Freundlich isotherm model was best fitted ($r^2 = 0.99734$–0.99955) among Langmuir, Dubinin–Radushkevich (D-R), and Temkin isotherms. The Langmuir monolayer adsorption capacity was 49.30966 mg/g at 30 °C. The adsorption mechanisms were supported by Reichenberg, Fick, Elovich, Furusawa, and Smith and Boyd models ($r^2 > 0.8$). The thermodynamics suggested endothermic, random, and spontaneous adsorption above 50 °C. The scale-up design using the Langmuir isotherm, and the disposal of used adsorbent after incineration, was established in this study. The research concludes that the red mud generated from the aluminum plant can be used to remove the phenol from wastewater.

Key words: adsorption, Freundlich isotherm, phenol, red mud, second-order kinetic, wastewater

Highlights

- Phenol pollutant could be removed from wastewater using low-cost red mud as adsorbent.
- Phenol removal percentage was studied with change of phenol conc., pH, time, dose and temperature.
- Kinetic study suggested that the process is chemical as the pseudo-second order model was fitted best.
- Isotherm study suggested that the process is chemical as the Freundlich model was most supportive.
- Red mud can be applied as a suitable adsorbent in industries with phenol removal efficiency of 87.5%.

Graphical Abstract

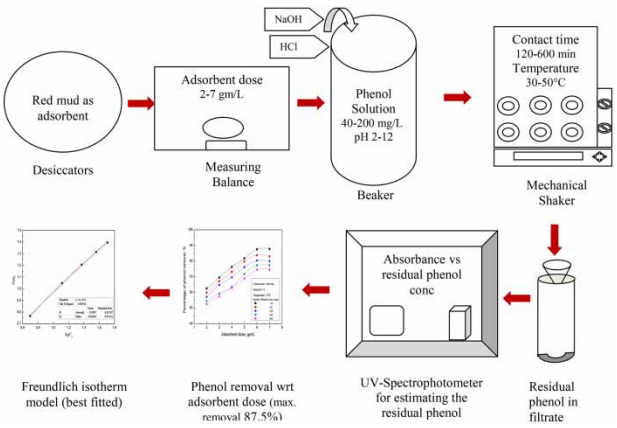

Water Practice & Technology Vol 15 No 3
doi: 10.2166/wpt.2020.056

NOMENCLATURE

a_1 Elovich constant
b Langmuir constant (L/mg)
B_1 Temkin constant connected with adsorption heat (J/mol)
b_1 Elovich constants
C_a Amount of phenol adsorbed on the adsorbent per liter of the solution at equilibrium (mg/L)
C_e Phenol concentration in solution at equilibrium (mg/L)
C_0 Initial phenol concentration in solution (mg/L)
C_t Phenol concentration in solution at time t (mg/L)
D_e Effective diffusion coefficient of adsorbate in the adsorbent phase (m^2/sec)
E Mean adsorption energy (kJ/mol)
$F(t)$ Ratio of the amount of Phenol adsorbed per gram of adsorbent at any time to that at equilibrium time
ΔG^0 Gibbs free energy (kJ/mol)
ΔH^0 Enthalpy (kJ/mole)
K_{ad} Pseudo-first-order rate constant (/min)
K' Pseudo-second-order rate constant (mg/g/min)
K_{bq} The constant obtained by multiplying q_{max} and b
$K_c^{/}$ Apparent equilibrium constant
K_c^0 Thermodynamic equilibrium constant
K_f Freundlich constant
K_T Equilibrium binding constant (L/g)
M Mass of the adsorbent per unit volume (g/L)
m_s Amount of adsorbent added (g)
n Freundlich constants intensity of adsorption (mg/g)/(mg/L)
q_e Amount of adsorbate (mg) adsorbed per gram of the adsorbent at equilibrium
q_{max} Maximum adsorption capacity (mg/g)
q_t Amount of adsorbate (mg) adsorbed per gram of adsorbent at time t
q_∞ Amount of adsorbate (mg) adsorbed per gram of adsorbent at infinity
r^2 Correlation coefficient
R Ideal gas constant (kJ/mol/K)
R_a Radius of the adsorbent particle (m)
R_L Separation factor
S_S External surface area of the adsorbent per unit volume (/m)
ΔS_0 Entropy (kJ/mol K)
t Time (min)
T Temperature (K)
t_o Elovich constant equals to $1/(a_1 b_1)$
V Volume of the solution (L)
X_m Maximum adsorption capacity of adsorbent (mill mol/g)
β Mass transfer coefficient (cm/sec)
λ Constant related to adsorption energy (in square mol/square kJ)
ε Polanyi potential (in square kJ/square mol)

INTRODUCTION

Phenol (C_6H_5OH) has been considered as a significant contaminant present in several domestic, agricultural, and industrial wastewaters (Mu'azu *et al.* 2017). It is treated as a severe human pollutant because of its high toxicity, since the toxicity leads to several chronic issues like anorexia, vomiting, fainting, kidney and liver damage, etc. (Busca *et al.* 2008). Phenol is treated as a severe environmental pollutant because it reduces soil porosity, affects the natural germination of seeds, and increases soil seepage, changing groundwater quality (Lakshmi *et al.* 2016). The impact owing to these contacts, however, varies with the quantum of phenol and its duration. Hence, phenol removal from its wastewater to an acceptable limit is necessary.

The industrial wastewater that contains phenol is usually discharged from industries like steel factories, oil refineries, coal-tar units, industrial resins, rubber plants, paint/disinfectant/pharmaceutical plants (Dargahi *et al.* 2017). Phenol can also be present in agricultural and domestic wastewater. The phenol content in industrial wastewater may group to the extent of 6,800 mg/L, whereas the

Water Practice & Technology Vol 15 No 3
doi: 10.2166/wpt.2020.056

permissible limit set by the EPA, USA, is 1.0 mg/L. Therefore the phenol quantum from wastewater must be reduced to this permissible limit before the wastewater is discharged into the surface water (Almasi *et al.* 2018). Although it is a significant pollutant in the wastewater, there are several other pollutants like metal ions, dye, etc. also prevailing in the wastewater, which can affect the water purification process.

Several methods are used to remove phenol from wastewater. They are solvent extraction, separation, flocculation, electro-Fenton, photo-degradation, oxidation, adsorption, etc. These methods are classified into physical, chemical, and biological types. Although there are many advantages associated with these methods, there are also certain disadvantages in many of them (Uddin *et al.* 2007). Many of these methods are not suitable because of the possibility of discharge of additional toxic materials or the high cost of the process (Naiya *et al.* 2009). The adsorption technique is usually considered as effective and eco-friendly (Divate & Hinge 2014). Although the activated carbons are generally considered the most efficient adsorbent, they are not favoured due to their high cost (Shokoohi *et al.* 2017). Therefore the applications of various natural adsorbents like algae, greensand, pumice, etc. are being investigated to replace activated carbon (Safari *et al.* 2015; Naghipour *et al.* 2016, 2018; Jaafari & Yaghmaeian 2019a, 2019b). The vital factor for choosing an adsorbent is, of course, a high surface area, microporous structure, and a high degree of surface reactivity (Sarkar & Das 2015, 2016). The applications of industrial and agricultural waste as adsorbents are studied through many researchers (Mandal *et al.* 2018, 2019a, 2019b, 2020; Mandal & Das 2019a, 2019b). Like the agricultural wastes, industrial wastes are also available in large quantities and almost free of cost. In this perspective, the red mud, industrial waste, is used as an adsorbent in this research. The porous structure of the red mud, having a high surface area, is usually supportive of adsorption. The presence of compounds like iron oxide, aluminum oxide, titanium oxide, calcium carbonate, sodium aluminum silicate, dicalcium silicate, and silicon oxide in red mud provides an enhanced binding spot for adsorption. The disposal of the used red mud is usually possible by incineration at a temperature above 800 °C, and its regeneration is not required since the red mud is generated in large quantities and is thus available almost free of cost. There is no cost involved in incineration as red mud, when used for brick manufacturing purposes, is required to be heated above 1,000 °C. The gradual increase of red mud applications for brick manufacturing purposes will thus reduce the disposal problem of the used adsorbents.

MATERIALS AND METHODS

Chemical and apparatus

The main apparatuses used were pH meter, Hach Germany; UV-Spectrophotometer, Hach Germany; scanning electron microscope (SEM), Hitachi Japan; X-ray diffractometer (XRD), Bruker Germany; Fourier transform infrared (FTIR) spectroscope, Thermo Fisher USA; BET, Quantachrome USA. A B.O.D. incubator shaker, heating furnace, and digital balance were also used for the experimentation. The chemicals, like analytical grade phenol (purity 99.99%), NaOH, and HCl from M/s Merck, India, were arranged for the experiments.

Adsorbent

The red mud was collected from NALCO, Damonjodi, Odisha, India. It is a by-product during alumina (aluminum oxide) production from bauxite. In general, 1.2–1.6 tonne of red mud is produced from 1 tonne of alumina production. The red mud was appropriately washed in distilled water and was kept for 8 hours at 110 °C in a furnace. It was then cooled at ambient condition, powdered in

Water Practice & Technology Vol 15 No 3
doi: 10.2166/wpt.2020.056

a grinder, and screened using −44 and +52 mesh sieves. The sieved quantity was then placed in a desiccator for batch experiments.

Characterizations of red mud

The surface topography assessed through the SEM apparatus is placed as Figure 1. The Figure 1 suggests that the red mud particle has numerous uneven pores. The SEM image further implied that the surface area of the red mud was high due to high porosity, with a relatively loose microstructure. Thus it was supportive of favourable adsorption.

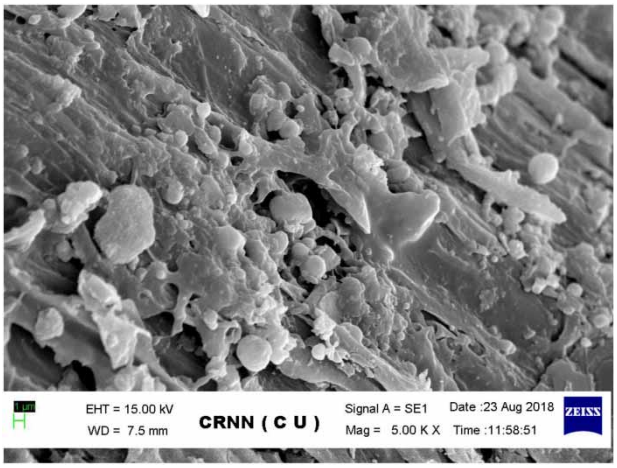

Figure 1 | The SEM topography of red mud.

The XRD spectra in Figure 2 suggest the presence of Fe_2O_3, $Al(OH)_3$, TiO_2, $CaCO_3$, $NaAlSiO_4$ Ca_2SiO_4, and SiO_2.

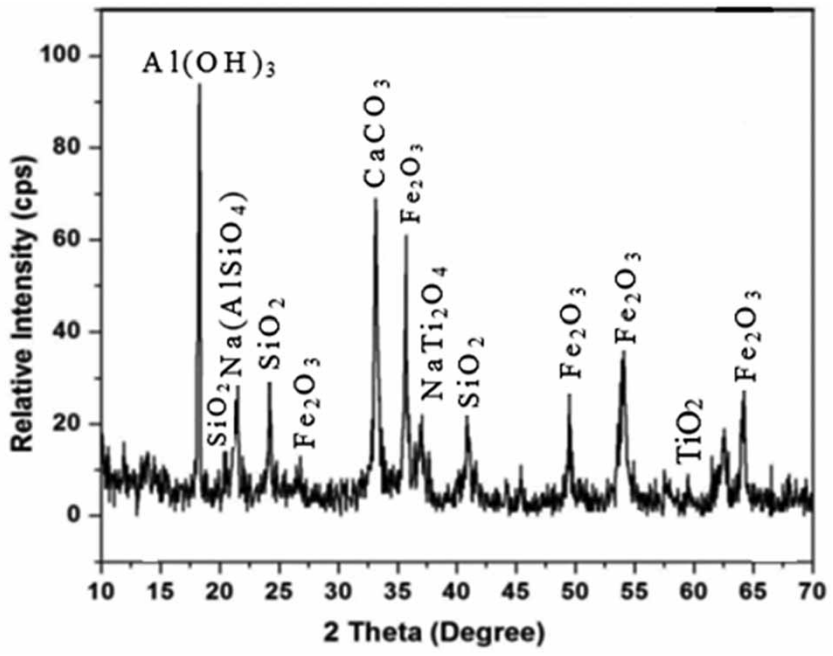

Figure 2 | The XRD spectra of red mud.

Water Practice & Technology Vol 15 No 3
doi: 10.2166/wpt.2020.056

The FTIR spectra in Figure 3 suggest that the 468 cm^{-1} and 521 cm^{-1} peaks were associated with Fe-O of Fe_2O_3. The peak at 560 cm^{-1} represented O-Si-O. The 730 cm^{-1} peak represented the Al–O bond. The 998 cm^{-1} peak corresponded to Si-O-Si in the silicate group. The band at 1,002 cm^{-1} was for Si–O–Si in the silicate group. The band at 1,410 cm^{-1} was described as the C = O stretching vibration and indicated the carbonate group. The peaks at around 3,415 cm^{-1}, 1,640 cm^{-1} and 2,850 cm^{-1} were assigned to the hydroxyl group vibration. The identified absorption band at 3,600–3,400 cm^{-1} corresponds with the vibration. These functional groups in red mud helped in chemical interactions through hydrogen bonding with the phenolate ions. The BET surface area was 300 m^2/g. The bulk density of the adsorbent was found to be 3 g/cm^3. The point of zero charge (pH_{pzc}) by the salt addition process was pH 7.65. The physical features and the chemical compositions of red mud are placed in Tables 1 and 2.

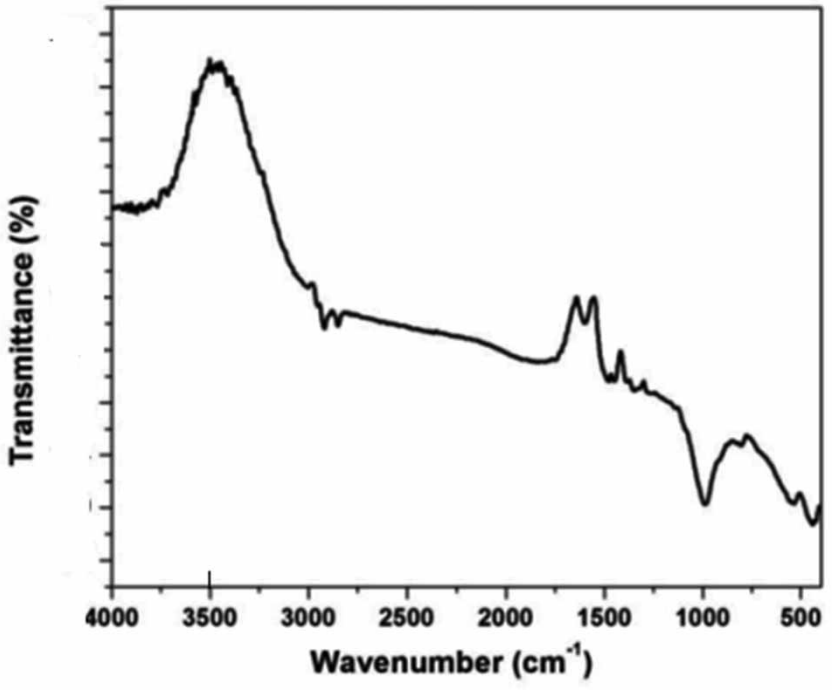

Figure 3 | The FTIR spectra of red mud.

Table 1 | Physical properties of red mud

Bulk density (g/cm^3)	Surface area (m^2/g)	Effective particle diameter (μm)	Point of zero charge
3.00	300	325	7.65

Table 2 | Typical chemical composition of red mud (collected from NALCO, Damanjodi authority)

Chemical composition	Range (wt %)
Fe_2O_3	48.2–53.8
Al_2O_3	17.7–19.8
SiO_2	4.8–5.7
Na_2O	3.8–4.6
TiO_2	3.6–4.2
CaO	0.8–1.2
Loss of ignition	10.8–11.3

Water Practice & Technology Vol 15 No 3
doi: 10.2166/wpt.2020.056

Preparation of aqueous phenol

The stock solution of aqueous phenol was prepared to take 1gm phenol (C_6H_5OH) in 1,000 ml double-distilled water. The concentration of this solution was 1,000 mg/L. This solution was diluted to prepare the desired concentration of phenol (40–200 mg/L). This procedure of dilution of the stock solution was considered to reduce the error in the weight measurement of a small quantity of crystal phenol required for desired low concentrations. The calibration chart was prepared using the absorbance values from the spectrophotometer corresponding to a known concentration of phenol. The same was used for the determination of the resultant phenol concentrations after adsorption.

Experimental

The phenol adsorption by red mud was tested in batch procedures with the variation of phenol content, pH, contact period, dose, and temperature. In every batch, 100 ml desired phenol solution (40–200 mg/L) was taken in 250 ml conical flask. The phenol concentration range of 40–200 mg/L was selected in this research work since the contaminant phenol available in the wastewater of many medium scale industries is in this range. The pH was varied from 2 to 12 using HCl and NaOH. The red mud dose was varied from 2 to 7 g/L. The temperature and contact time were maintained at 30–50 °C and 120–600 min using a thermostatic shaker at 120 strokes/minute. At the end of the experiment, the absorbance of the filtrate was measured in the UV-spectrophotometer, and the residual phenol content was checked using the calibration curve. The experiments were repeated thrice, and the average was accounted for more precision. Reproducibility and relative variance were found to be $\pm 0.5\%$ and $\pm 0.25\%$, respectively. The standard deviation of the variance was shown in the relevant graphical presentation.

The phenol removal was computed using Equation (1).

$$\% \text{ of phenol removal} = \frac{(C_0 - C_t)}{C_0} \times 100\% \tag{1}$$

The phenol adsorbed in red mud was computed by the Equation (2).

$$q_t = \frac{(C_0 - C_t)}{m_s} \tag{2}$$

RESULTS AND DISCUSSION

Variation of time

The batch tests were conducted with the variation of time (120–600 min) and phenol concentration (40–200 mg/L). The pH, dose, and temperature were unchanged at 8, 6 g/L, and 50 °C. The phenol removal versus time was as shown in Figure 4. The graph described that the removal increased in the beginning and then became constant after 480 min. Similar results were found for all phenol concentrations (40–200 mg/L). The removal was faster initially as the adsorbent had empty sites. Meanwhile, the oxides and silica present in red mud took part in the adsorption, and the oxygenated surface of the adsorbent facilitated the adsorption by hydrogen bonding with the hydroxyl surface of the phenol. However, when the equilibrium arrived at 480 min, regardless of phenol concentration the adsorption sites became saturated and therefore, after that, no more adsorption was possible.

Water Practice & Technology Vol 15 No 3
doi: 10.2166/wpt.2020.056

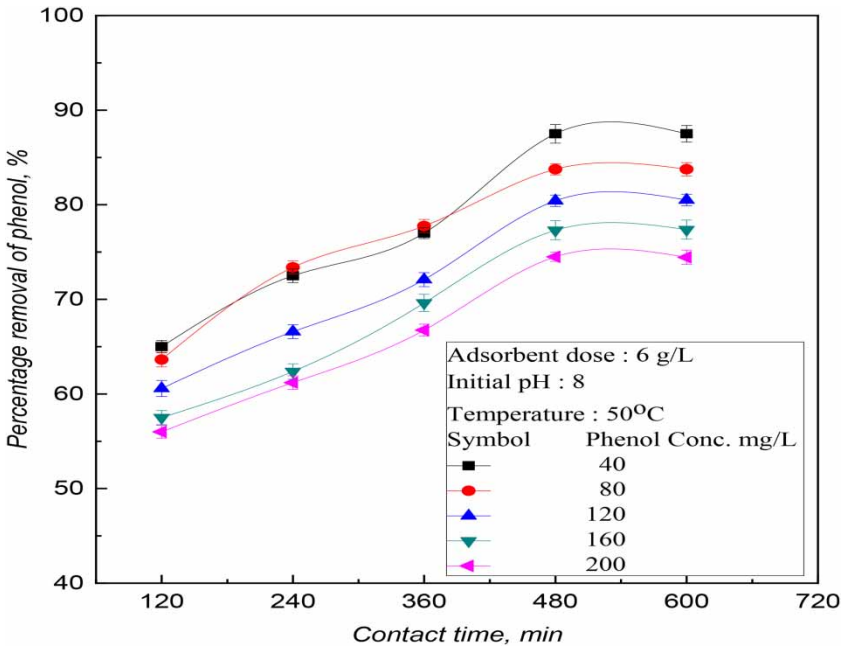

Figure 4 | The effect of contact time for phenol removal.

The decrease of phenol removal with the increase of the initial phenol concentration can be explained as the red mud has a limited number of active sites; and can be quickly saturated (Tor *et al.* 2006).

Variation of dose

The experiments were conducted with the variation of dose (2–7 g/L) and phenol contents (40–200 mg/L). The pH, time, and temperature were unchanged at 8, 480 min, and 50 °C. The phenol removal versus dose is shown in Figure 5. The graph describes that the removal increased in the

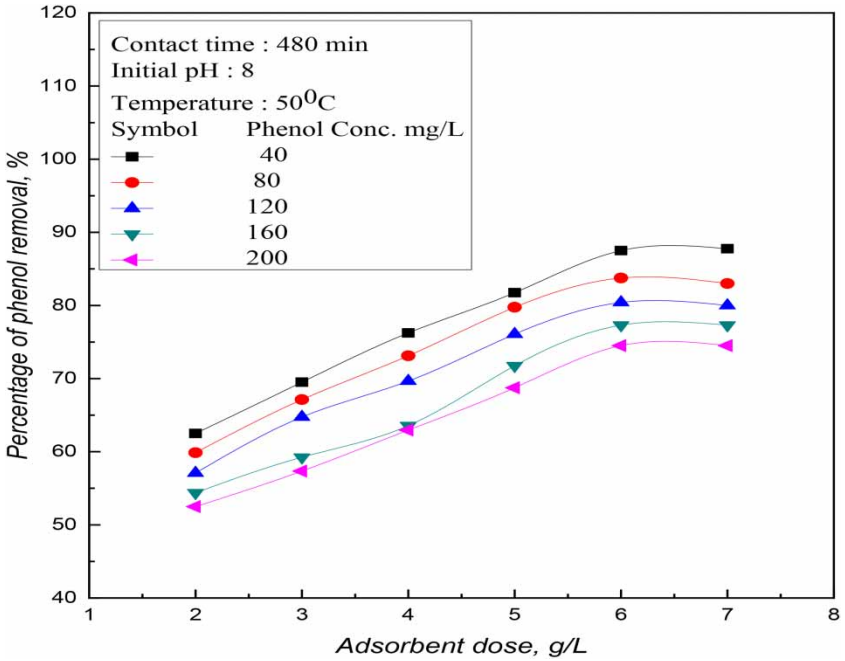

Figure 5 | The effect of adsorbent dose for phenol removal.

Water Practice & Technology Vol 15 No 3
doi: 10.2166/wpt.2020.056

beginning and then became constant after the dose of 6 g/L. Similar results were found for all phenol concentrations (40–200 mg/L). The removal was faster initially, as the adsorbent had empty sites. The higher rate of adsorption continued because of the addition of surface area through the continued addition of adsorbent. This phenomenon was observed up to the adsorbent dose of 6 g/L. However, the addition of more quantity of adsorbent beyond 6 g/L was not required because the active adsorbent sites got saturated, and the adsorbent sites were overlapped due to overcrowding of red mud particles.

Variation of pH

The experiments were conducted with the variation of pH (2–12) and phenol contents (40–200 mg/L). The dose, time, and temperature were unchanged at 6 g/L, 480 min, and 50 °C. The phenol removal versus pH is shown in Figure 6. Similar results were found for all phenol concentrations (40–200 mg/L). The graph showed an increase in phenol removal with pH 2–8. After pH 8, the removal, however, decreased considerably. Hence, the optimum pH was 8. The reason for this observation was the amphoteric properties of red mud at the point of zero charge (pH_{pzc}) 7.65. The amphoteric behaviour was due to the zero surface charge at pH 7.65 when the adsorbent came in contact with water. The functional groups present in the adsorbent played a significant role in such amphoteric characteristics. The pK_a value of phenol is 9.9, which indicates that the phenol is a weak acid and exists as anions at higher pH. As the pH of the solution surpasses the pK_a, the phenol exists as phenolate ions, and at below the pK_a value, it exists as a neutral molecule (Kumar *et al.* 2014). The pH_{PZC} values of Fe_2O_3, Al_2O_3, CaO, and SiO_2 are 8.5, 8.3, 11.0, and 2.2, respectively. The optimum pH is 8; hence, for $pH \leq pH_{PZC}$ an electrostatic attraction exists between the positively charged surface of the red mud and the phenolate ion. At $pH \geq 9$, the red mud surface and phenolate anions will repel each other because of the negative surface charge of Fe_2O_3, Al_2O_3, the significant component in the red mud. At low pH, that is, the acidic solution that causes extra protons to exist in the solution, there will be a competition between the protons and phenol, hence the significant drop in adsorption (Halouli & Drawish 1995; Nagda *et al.* 2007).

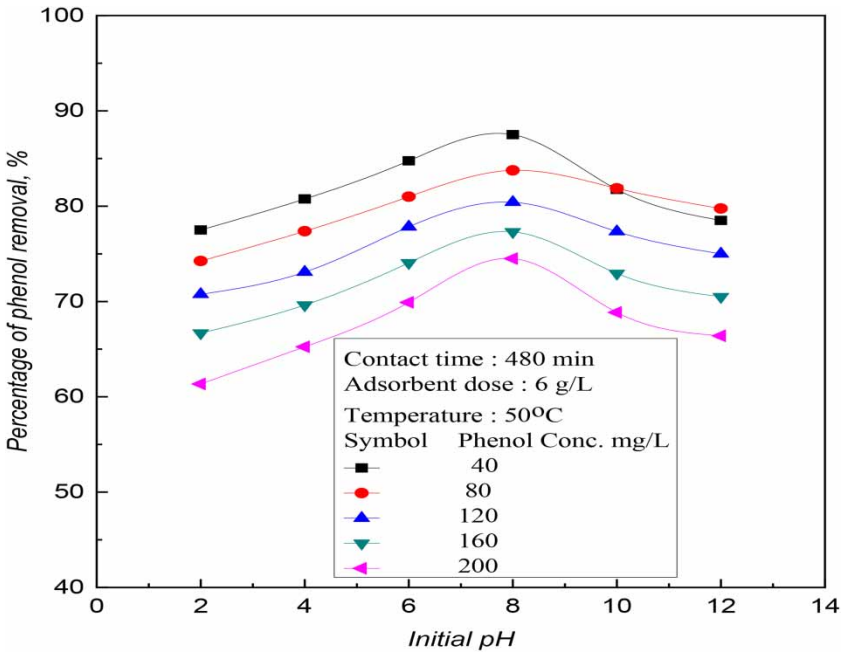

Figure 6 | The effect of pH for phenol removal.

Water Practice & Technology Vol 15 No 3
doi: 10.2166/wpt.2020.056

Variation of temperature

The tests were conducted with the variation of temperature 30–50 °C) and phenol contents (40–200 mg/L). The pH, time, and dose were unchanged at 8, 480 min, and 6 g/L. The phenol removal versus temperature is shown in Figure 7. Similar results were found for all phenol concentrations (40–200 mg/L). The intra and intermolecular hydrogen bond becomes weak at a higher temperature; hence, phenol molecules are freely available for adsorption (Gupta *et al.* 2004). The graph describes that the removal increased with temperature because of better chemical interaction between red mud and phenol due to the increase of electrostatic forces. At higher temperatures, the mass transfer rate from the bulk to the boundary layer around the red mud surface increases due to a decrease in the boundary layer thickness. This enhances the rate of chemical reaction, hence adsorption capacity increases, and the adsorption process is chemical. The reduction of Gibbs free energy evaluated by thermodynamic analysis also supported better chemical interaction at the higher temperature. Hence, the adsorption was endothermic (Ekpete *et al.* 2010).

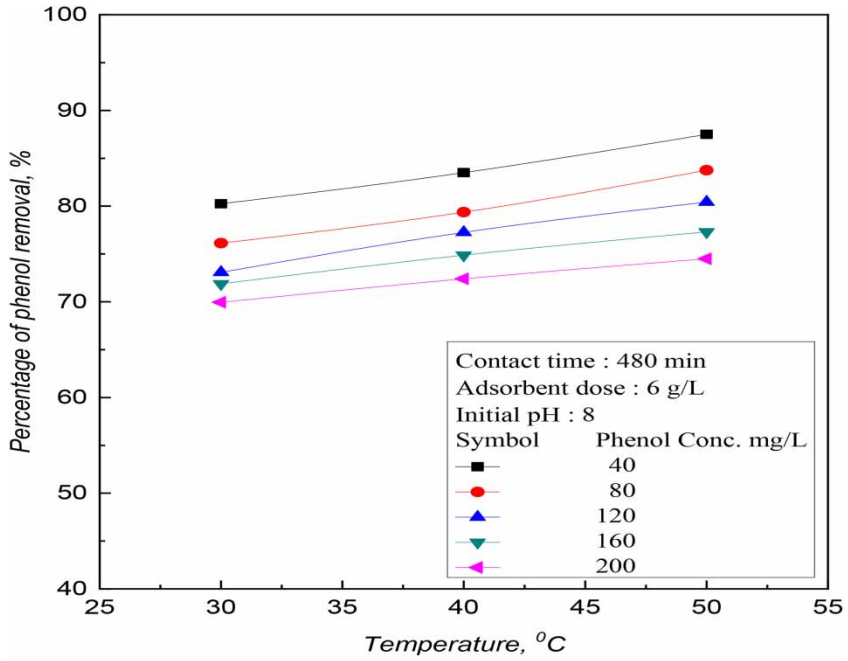

Figure 7 | The effect of temperature for phenol removal.

Kinetic study

The phenol removal rate with time was studied using different phenol contents (40–200 mg/L) at constant pH, dose, and temperature. The results showed maximum phenol removal at 480 min. These results were tested using seven kinetic models.

Pseudo-first-order model

The model (Lagergren 1898) can be described as in Equation (3).

$$\log(q_e - q_t) = \log q_e - \frac{K_{ad}}{2.303}t \tag{3}$$

Water Practice & Technology Vol 15 No 3
doi: 10.2166/wpt.2020.056

This model suggests physisorption with the homogeneous surface of the adsorbent involving Van Der Waal forces of attraction. The model parameters were calculated from the graph of $\log(q_e - q_t)$versus t. The higher the value of rate constant K_{ad}, the faster the rate of adsorption, and the higher the value of q_e, the higher the amount of phenol that is adsorbed by red mud in equilibrium.

Pseudo-second-order model

The model is described as in Equation (4).

$$\frac{t}{q_t} = \frac{1}{K' q_e^2} + \frac{t}{q_e} \tag{4}$$

This model suggests chemisorption with the heterogeneous surface of the adsorbent involving chemical bonding forces of attraction (Chaudhary *et al.* 2014). The parameters were calculated from the graphs $\frac{t}{q_t}$ against t. The higher the value of rate constant K', the faster will be the rate of chemical adsorption and the higher the value of q_e, the higher will be the amount of phenol uptake capacity by red mud in equilibrium.

The results of pseudo kinetic models reported in Table 3 indicated that the pseudo-second-order model was better statistically. Table 3 also shows that the derived quantities of q_e for the pseudo-second-order model were more proximate than the experimental q_e. Therefore, the adsorption method would be chemical and heterogeneous (Singha & Das 2012).

Table 3 | Comparison of pseudo first-order and pseudo second-order results

		Pseudo first order model			Pseudo second order model		
C_o (mg/L)	$q_{e,\ exp}$ (mg/g)	K_{ad} (1/min)	$q_{e,\ cal}$ (mg/g)	r^2	K' (g/mg min)	$q_{e,\ cal}$ (mg/g)	r^2
40	5.83333	0.00317	2.17801	0.99727	0.00465	5.65611	0.99918
80	11.16667	0.00504	4.82114	0.99401	0.00189	11.66045	0.99994
120	16.08333	0.00359	6.27682	0.98144	0.00153	15.92864	0.99599
160	20.61667	0.00391	9.04086	0.89751	0.00100	20.75550	0.98665
200	24.83333	0.00363	9.86166	0.96162	0.00096	24.63054	0.99407

Reichenberg model

The Reichenberg model (Reichenberg 1953), which is used to check the biosorption process, either film or intra-particle diffusion is expressed as in Equation (5).

$$Bt = -0.4977 \ln[1 - F(t)] \tag{5}$$

The conformity of this model could be established by studying their correlation coefficients after the graphs are plotted using the values of Bt against t. The support of this model suggests film diffusion, and the higher the diffusion rate constant Bt, the faster the rate of film diffusion will be through mass transfer. The plot is a straight line but not passing through the origin, indicating the film diffusion-controlled process (Gupta 1998).

Water Practice & Technology Vol 15 No 3
doi: 10.2166/wpt.2020.056

Fick model

This model, signifying the diffusion between phenol and red mud, is indicated as

$$\frac{q_t}{q_\alpha} = \frac{6}{R_a}\sqrt{\frac{D_e t}{\pi}} \tag{6}$$

This model can be analyzed using graphs of q_t/q_e versus t. If the linear plot of the figure shows a single line, the process will have intra-particle diffusion. The first straight line will signify film diffusion if the figure shows two or more multi-linear lines after linearization. The second will signify pore diffusion, and the third will mean intraparticle diffusion. The corresponding time for each type of diffusion can be evaluated from the graph. The involvement of maximum time will decide the rate-determining step occurring in the adsorption process. The ratio of film diffusion time to intra-particle diffusion time was found to be 1:1; hence, the process was regulated jointly by film and intra-particle diffusion.

Furusawa and Smith model

This model, which signified towards the mass transfer mechanism in the adsorption process, can be expressed as in Equation (7).

$$\ln\left(\frac{C_t}{C_0} - \frac{1}{1+MK_{bq}}\right) = \ln\left(\frac{MK_{bq}}{1+MK_{bq}}\right) - \left(\frac{1+MK_{bq}}{MK_{bq}}\right)\beta S_S t \tag{7}$$

Here, the K_{bq} was evaluated by the product of b and q_{max} evaluated from the Langmuir isotherm. From the graph of $\ln\left(\frac{C_t}{C_0} - \frac{1}{1+MK_{bq}}\right)$ versus t, the parameters were estimated. This model used for mass transfer mechanism is developed for external film diffusion during the initial adsorption process. The coefficient of mass transfer, β, can be calculated from the graphs for estimating whether phenol movement from solution to the adsorbent surface is faster. The higher the value of mass transfer rate constant β, the quicker will be the rate of phenol movement through external film diffusion.

Elovich model

This model, signifying chemisorption, can be described as in Equation (8).

$$q_t = \frac{1}{b_1}\ln(a_1 b_1) + \frac{1}{b_1}\ln(t + t_0) \tag{8}$$

This model is tested using graph q_t versus lnt. The higher the value of rate constant a_1, the faster will be the rate of adsorption, and the higher the value of b_1, the higher will be the rate of desorption.

Boyd model

This model (Boyd *et al.* 1947) signifying chemisorption can be described as in Equation (9).

$$\ln\left[\frac{1}{1-F^2(t)}\right] = \frac{\pi^2}{R_a^2} D_e t \tag{9}$$

Water Practice & Technology Vol 15 No 3
doi: 10.2166/wpt.2020.056

This model can be tested using graph $\ln\left[\frac{1}{1-F^2(t)}\right]$ and t. If the external mass transfer is greater than the internal one, film diffusion controls, and if the internal mass transfer is greater than the external one, particle diffusion controls. This can be verified from the linear plot of the graph. In the case of a linear plot passing through the origin, particle diffusion controls or else film diffusion controls. The diffusion coefficient, D_e, can then be derived from the plot. The process will be chemical if D_e falls between 10^{-9} and 10^{-17} m^2/sec.

The results of kinetic testing are reported in Table 4. The Reichenberg model suggested film diffusion, whereas the Fick model indicated that the film and intra-particle diffusion were both equally important. The Furusawa and Smith model suggested faster phenol movement. The Elovich model and the Boyd model suggested the chemisorption process.

Table 4 | Kinetic model results

Kinetic model	Initial phenol conc. (mg/L)	Correlation coefficient	Critical values	Result
Reichenberg model	40	0.99727	–	Since the value of correlation coefficient is above 0.8, the adsorption process is of film diffusion
	80	0.99401		
	120	0.98114		
	160	0.89713		
	200	0.96188		
Fick model	40	0.85138	–	The linear segments of the curve implied that the film diffusion and intraparticle diffusion take 240 min each
	80	0.96143		
	120	0.94485		
	160	0.99129		
	200	0.95862		
Furusawa and Smith model	40	0.80328	$\beta = 1.443 \times 10^{-11}$ cm/sec	The value of correlation coefficient above 0.8 suggests that phenol moves faster from bulk to solid stage
	80	0.92623	$\beta = 2.686 \times 10^{-12}$ cm/sec	
	120	0.91017	$\beta = 2.296 \times 10^{-12}$ cm/sec	
	160	0.91821	$\beta = 1.945 \times 10^{-12}$ cm/sec	
	200	0.91836	$\beta = 1.527 \times 10^{-12}$ cm/sec	
Elovich model	40	0.91825	–	The value of correlation coefficient above 0.8 supports that the adsorption process is chemical
	80	0.97684		
	120	0.92974		
	160	0.91792		
	200	0.92666		
Boyd model	40	0.99885	$D_e = 1.276 \times 10^{-13}$ m^2/sec	The value of the diffusion coefficient being within 10^{-9} and 10^{-17} supports that the process is chemisorption
	80	0.99674	$D_e = 2.080 \times 10^{-13}$ m^2/sec	
	120	0.97571	$D_e = 1.468 \times 10^{-13}$ m^2/sec	
	160	0.88583	$D_e = 1.602 \times 10^{-13}$ m^2/sec	
	200	0.95448	$D_e = 1.473 \times 10^{-13}$ m^2/sec	

Isothermal study

The phenol removal was tested at different temperatures and phenol contents (40–200 mg/L) with constant pH, dose, and time. The results suggested that the phenol removal was increased with temperature and indicated the endothermic chemical reaction. The isotherm study was performed using four models.

Langmuir model

This model (Langmuir 1918) is described by Equation (10).

$$\frac{C_e}{q_e} = \frac{1}{q_{\max} b} + \frac{C_e}{q_{\max}} \tag{10}$$

Water Practice & Technology Vol 15 No 3
doi: 10.2166/wpt.2020.056

The q_{max} and b are calculated from the graph $\frac{C_e}{q_e}$ against C_e. The higher the value of q_{max}, the higher will be the monolayer adsorption capacity and the larger value of b will suggest larger free adsorption energy. The Langmuir model supports that the adsorbent surface is homogeneous, suggesting no lateral interaction between the adsorbed particles on the surface of red mud. The separation factor, R_L, is used to predict the affinity between phenol and red mud using the Langmuir constant. In this perspective, this isotherm can be re-expanded further to decide the value of separation factor R_L applying Equation (11).

$$R_L = \frac{1}{1 + bC_0} \tag{11}$$

The Langmuir model is favourable if R_L lies between 0 and 1.

Freundlich model

This model (Freundlich 1906) is described by Equation (12).

$$\log q_e = \log K_f + \frac{1}{n} \log C_e \tag{12}$$

From the graph of log q_e against log C_e, K_f and $\frac{1}{n}$ are derived. The higher the value of K_f, the higher will be the multilayer adsorption capacity and the higher the value of n, the higher will be the adsorption's free energy. The Freundlich model supports that the adsorbent surface is heterogeneous, suggesting multilayer adsorption over a large number of available sites acting simultaneously. The values of $\frac{1}{n}$ between 0 and 1 indicate heterogeneous adsorption.

Temkin model

This model has been developed (Temkin & Pyzhev 1940) by Equation (13).

$$q_e = B_1 \ln K_T + B_1 \ln C_e \tag{13}$$

From the graph of q_e against lnC_e, the parameters B_1 and K_T can be evaluated. The Temkin constants B_1 and K_T signify adsorption heat and equilibrium binding energy, respectively.

Dubinin–Radushkevich (D-R)

This model can be expressed by Equations (14) and (15).

$$\ln q_e = \ln X_m - \lambda \varepsilon^2 \tag{14}$$

$$\varepsilon = RT \ln \left(1 + \frac{1}{C_e}\right) \tag{15}$$

The graphs for $\ln q_e$ against ε^2 will give the quantities of λ and X_m. The lower the value of λ, the higher will be the adsorption energy and the higher the value of X_m, the higher will be the adsorption capacity. Using λ value the sorption energy (E) can be evaluated from Equation (16).

$$E = \frac{1}{\sqrt{2\lambda}} \tag{16}$$

Water Practice & Technology Vol 15 No 3
doi: 10.2166/wpt.2020.056

The process supports physisorption if E is below 8 and supports chemisorption if E is between 8 and 16. The results of isotherm model parameters are reported in Table 5. Table 5 shows the highest correlation coefficient for the Freundlich model for all the temperature range from 30 °C to 50 °C. The sorption energy, E, varies from 0.2009 to 1.7557 kJ/mol. It indicated the process was physical adsorption, but the correlation coefficient was low ($r^2 < 0.8$), so not acceptable. Table 5 also shows that the maximum adsorption capacity varies from 49.3 mg/g to 39.1 mg/g, and the temperature ranges from 30 °C to 50 °C.

Table 5 | Isotherm model parameters

	30°C		40°C		50°C	
Isotherm model	**Correlation coefficient**	**Isotherm constants**	**Correlation coefficient**	**Isotherm constants**	**Correlation coefficient**	**Isotherm constants**
Langmuir isotherm	0.93185	q_{max} (mg/g) 49.30966 b (L/mg) 0.01416	0.96919	q_{max} (mg/g) 46.08295 b (L/mg) 0.01922	0.98026	q_{max} (mg/g) 39.10833 b (L/mg) 0.03193
Freundlich isotherm	0.99955	K_f 1.18749 n 1.37538	0.99884	K_f 1.50244 n 1.43211	0.99734	K_f 2.18625 n 1.60046
Temkin isotherm	0.93669	B_1 (J/mol) 8.66953 K_T (L/g) 0.20108	0.95250	B_1 (J/mol) 8.67652 K_T (L/g) 0.24775	0.96457	B_1 (J/mol) 8.08288 K_T (L/g) 0.35779
Dubinin–Radushkevich isotherm	0.77774	X_m (mg/g) 17.92883 E (kJ/mol) 0.2009	0.78002	X_m (mg/g) 18.60945 E (kJ/mol) 0.2381	0.78524	X_m (mg/g) 1.62889 E (kJ/mol) 1.7557

Thermodynamic study

The tests were conducted at different temperatures (30–50 °C) and phenol content (40–200 mg/L) with constant pH, dose, and time. The results showed an increase in phenol removal with temperature. The phenol removal percentage varied from 80.25% to 87.50% for a phenol concentration of 40 mg/L, from 76.13% to 83.75% for 80 mg/L, from 73.08% to 80.42% for 120 mg/L, from 71.88% to 77.31% for 160 mg/L and from 69.95% to 74.50% for 200 mg/L for 30, 40 and 50 °C respectively. The reasons for higher phenol removal at higher temperatures were probably the widening of adsorbent pores and the higher mobility of phenolate ions. The thermodynamic equilibrium constant, K_c^0, was obtained by calculating the apparent equilibrium constant, $K_c^{/}$, at different temperatures and initial phenol concentration for each system and extrapolating to zero (Dakiky *et al.* 2002; Singha & Das 2013).

$$K_c^{/} = \frac{C_a}{C_e} \tag{17}$$

The experimental results were used for the calculation of free energy, entropy, and enthalpy using Equations (18)–(20).

$$\Delta G^o = -RT \ln K_c^0 \tag{18}$$

$$\ln K_c^0 = -\frac{\Delta H^o}{RT} + \frac{\Delta S^o}{R} \tag{19}$$

$$\Delta G^o = \Delta H^o - T\Delta S^o \tag{20}$$

Water Practice & Technology Vol 15 No 3
doi: 10.2166/wpt.2020.056

The plot of $\ln K_c^0$ against $\frac{1}{T}$ determines the values of ΔG^o, ΔS^o, and ΔH^o, which are reported in Table 6. The values of ΔG^o being negative, the adsorption process was spontaneous. The positive ΔH^o supported an endothermic reaction. The positive ΔS^o suggested a higher degree of randomness in the adsorption process.

Table 6 | Values of ΔG^0, ΔH^0 and ΔS^0

T (K)	ΔG^0 (kJ/mol)	ΔH^0 (kJ/mol)	ΔS^0 (kJ/mol K)
303	−3.48407		
313	−4.15046	20.67691	0.07959
323	−5.08178		

Adsorption mechanism

The adsorption mechanism is summarized as follows:

i. Pore capture: the SEM image shows that the red mud is very porous and consists of many uneven pores. The phenol adsorption takes place on the pores of the red mud.
ii. Hydrogen bonding: oxygen-containing functional groups, as identified by FTIR spectra, promote the phenol adsorption by hydrogen bond formation by the interactions between the red mud surface and phenol. The peak in the FTIR (Figure 3) at 2,850 cm^{-1} corresponds to the –OH group present on the red mud surface. The intermolecular hydrogen bonding between phenol and red mud increases the adsorption.
iii. Electrostatic interaction: The constitution of red mud is of different metal oxides. There is the formation of the metal-phenol complex onto the hydrous metal oxide. It is due to the ligand exchange process between the phenol and hydroxyl group on the red mud surface. The pH_{PZC} values of Fe_2O_3, Al_2O_3, CaO, and SiO_2 are 8.5, 8.3, 11.0, and 2.2, respectively. The optimum pH is 8; hence, for $pH \leq pH_{PZC}$, electrostatic attraction exists between the positively charged surface of the red mud and the phenolate ion.

Comparison of adsorption capacity

The comparison of the maximum adsorption capacity for phenol removal by different adsorbents and the present study is shown in Table 7. Red mud has comparable adsorption capacity and therefore is suitable for practical use. The low cost and the vast availability of red mud are the added advantages for its selection by many industries.

SCALE-UP DESIGN

The Langmuir isotherm was used for the scale-up design in this adsorption process. Equation (2) is reproduced as in Equation (21).

$$q_t = \frac{(C_0 - C_t)}{m_s} = \frac{(C_0 - C_t)V}{W} \tag{21}$$

Water Practice & Technology Vol 15 No 3
doi: 10.2166/wpt.2020.056

Table 7 | Comparison of maximum adsorption capacity for phenol removal

Adsorbent	q_{max} (mg/g)	pH	Temperature (°C)	Time (min)	Reference
Activated carbon	49.720	–	–	–	Ozkaya (2006)
Neutralized red mud	4.127	6	25	600	Tor *et al.* (2006)
HDTMA-kaolinite	3.972	–	–	–	Alkaram *et al.* (2009)
Acacia tortilis pod shell	21.320	2	45	10	Malakootian *et al.* (2018)
AC from coconut coir	980.39	6	30	250	Mandal *et al.* (2018)
Clarified sludge from BOF	1.052	7	35	240	Mandal & Das (2019a)
Activated alumina	51.867	3	30	120	Mandal & Das (2019b)
Rice husk ash	13.982	9	35	180	Mandal *et al.* (2019a)
Rice husk	50.150	5	35	240	Mandal *et al.* (2019b)
Guava tree bark	44.702	7	50	120	Mandal *et al.* (2020)
Red mud	49.309	8	30	480	This study

At equilibrium, Equation (21) is modified to Equation (22).

$$\frac{W}{V} = \frac{(C_o - C_t)}{q_t} = \frac{(C_o - C_t)}{q_e} \tag{22}$$

Using the Langmuir isotherm model, Equation (22) is modified as in Equation (23).

$$\frac{W}{V} = \frac{(C_o - C_t)}{q_e} = \frac{(C_O - C_t)}{(C_e q_{\max} b)/(1 + bC_e)} \tag{23}$$

Equation (23) is applied for scale-up design, and the weight of red mud (g) required for phenol removal is shown in Table 8.

Table 8 | Required weight of adsorbent (g) for different volume of wastewater (L)

Volume of wastewater (L)	80% Adsorption	60% Adsorption	40% Adsorption	20% Adsorption
2	11.89	8.91	5.94	2.97
4	23.77	17.83	11.89	5.94
6	35.66	26.74	17.83	8.91
8	47.54	35.66	23.77	11.89
10	59.43	44.57	29.71	14.86

DISPOSAL OF USED ADSORBENT

The red mud used as adsorbent was generated at the bauxite refinery plant as a waste by-product. It is available at little cost, its regeneration is also not significant, and the researchers do not insist on any desorption technique for reuse of such adsorbents. The used adsorbents were destroyed by incineration at 800 °C. The incinerated ash is suitable for rood making or land-filling. The used adsorbents are also suitable as one ingredient for the production of bricks, which requires above 1,000 °C.

CONCLUSION

The phenol removal rate on red mud was investigated in this research. The surface characterizations of red mud were carried out. The batch tests were conducted with phenol content (40–200 mg/L), pH

Water Practice & Technology Vol 15 No 3
doi: 10.2166/wpt.2020.056

(2–12), time (120–600 min), dose (2–7 g/L), and temperature (30–50 °C). The maximum removal (87.5%) was obtained at pH 8, time 480 min, and dose 6 g/L. The adsorption kinetic was the pseudo-second-order. The Reichenberg model supported film diffusion, and the Fick model supported the equal importance of film and intra-particle diffusions. The Furusawa and Smith model suggested rapid phenol movement to the adsorbent surface. Both Boyd and Elovich models suggested chemisorption. The Freundlich model was the best-fitted isotherm model among Langmuir, Temkin, and Dubinin–Radushkevich models. The process was endothermic, random, and spontaneous. The mechanism of adsorption involved in the phenol removal process was deliberated with conclusive explanations. The safe dumping of used red mud was tested by incineration. The scale-up design was calculated to find the quantity of adsorbent required for phenol removal. The study concludes that red mud is suitable for phenol removal from wastewater.

CONFLICT OF INTEREST

The authors have no conflict of interest to disclose.

DATA AVAILABILITY STATEMENT

Data cannot be made publicly available; readers should contact the corresponding author for details.

REFERENCES

Alkaram, U. F., Mukhlis, A. A. & Al-Dujaili, A. H. 2009 The removal of phenol from aqueous solutions by adsorption using surfactant-modified bentonite and kaolinite. *Journal of Hazardous Materials* **169**, 324–332.

Almasi, A., Dargahi, A., Amrane, A., Fazlzadeh, M., Soltanian, M. & Hashemian, A. 2018 Effect of molasses addition as biodegradable material on phenol removal under anaerobic conditions. *Environmental Engineering and Management Journal* **17**(6), 1475–1482.

Boyd, G. E., Adamson, A. W. & Myers, L. S. 1947 The exchange adsorption of ions from aqueous solutions by organic zeolites. II. Kinetic. *Journal of American Chemical Society* **69**, 2836–2848.

Busca, G., Beradinelli, S., Resini, C. & Arrighi, L. 2008 Technologies for the removal of phenol from fluid streams. *Journal of Hazardous Materials* **160**, 265–288.

Chaudhary, N., Balomajumder, C., Agrawal, B. & Jagati, V. S. 2014 Removal of phenol using fly ash and impregnated fly ash: an approach to equilibrium, kinetic and thermodynamic study. *Separation Science and Technology* **50**, 690–699.

Dakiky, M., Khamis, M., Manassra, A. & Mer'eb, M. 2002 Selective adsorption of chromium(VI) in industrial wastewater using low-cost abundantly available adsorbents. *Advances in Environmental Research* **6**, 533–540.

Dargahi, A., Mohammadi, M., Amirian, F., Karami, A. & Almasi, A. 2017 Phenol removal from oil refinery wastewater using anaerobic stabilization pond modelling and process optimization using response surface methodology (RSM). *Desalination and Water Treatment.* **87**, 199–208.

Divate, S. B. & Hinge, R. V. 2014 Review on research removal of phenol from wastewater by using different methods. *International Journal of Scientific and Research Publications* **4**(5), 1–3.

Ekpete, O. A., Horsfall, M. & Tarawou, T. 2010 Potential of fluid and commercial activated carbons for phenol removal in aqueous systems. *American Journal of Applied Sciences* **5**(9), 39–47.

Freundlich, H. 1906 Adsorption in solution. *The Journal of Physical Chemistry* **57**, 384–410.

Gupta, V. K. 1998 Equilibrium uptake, sorption dynamics, process development, and column operations for the removal of copper and nickel from aqueous solution and wastewater using activated slag, a low-cost adsorbent. *Industrial and Engineering Chemistry Research* **37**, 192–202.

Gupta, V. K., Ali, I. & Saini, V. K. 2004 Removal of chlorophenols from wastewater using red mud: an aluminium industry waste. *Environmental Science and Technology* **38**, 4012–4018.

Halouli, K. A. & Drawish, N. M. 1995 Effects of pH and inorganic salts on the adsorption of phenol from aqueous systems on activated decolourising charcoal. *Separation Science and Technology* **30**, 3313–3324.

Jaafari, J. & Yaghmaeian, K. 2019a Response surface methodological approach for optimizing heavy metal biosorption by the blue-green alga Chroococcus disperses. *Desalination and Water Treatment* **142**, 225–234.

Jaafari, J. & Yaghmaeian, K. 2019b Optimization of heavy metal biosorption onto fresh water algae (*Chlorella coloniales)* using response surface methodology (RSM). *Chemosphere* **217**, 447–455.

Water Practice & Technology Vol 15 No 3
doi: 10.2166/wpt.2020.056

Kumar, N. S., Hasfalina, C. M. & Woo, H.-S. 2014 Biosorption of phenolic compounds from aqueous solutions using pine (*Pine densiflorasieb*) bark powder. *Bioresources* **9**(3), 5155–5174.

Lagergren, S. 1898 About the theory of so-called adsorption of soluble substances. *Handlingar* **24**, 1–39.

Lakshmi, S., Harshitha, M., Vaishali, G., Keerthana, S. R. & Muthappa, R. 2016 Studies on different methods for removal of phenol in waste water: review. *International Journal of Science, Engineering and Technical Research* **5**(7), 2488–2496.

Langmuir, I. 1918 The adsorption of gases on plane surfaces of glass, mica and platinum. *Journal of the American Chemical Society* **40**, 1361–1403.

Malakootian, M., Mahvi, A. H., Mansoorian, H. J. & Khanjani, N. 2018 Agrowaste based ecofriendly bio-adsorbent for the removal of phenol: adsorption and kinetic study by acacia tortilis pod shell. *Chiang Mai Journal of Science* **45**(1), 355–368.

Mandal, A. & Das, S. K. 2019a Phenol adsorption from wastewater using clarified sludge from basic oxygen furnace. *Journal of Environmental Chemical Engineering* **7**(4), 103259.

Mandal, A. & Das, S. K. 2019b Adsorptive removal of phenol by activated alumina and activated carbon from coconut coir and rice husk ash. *Water Conservation Science and Engineering* **44**(4), 149–161.

Mandal, A., Mukhopadhyay, P. & Das, S. K. 2018 Removal of phenol from aqueous solution using activated carbon from coconut coir. *IOSR Journal of Engineering* **8**(12), 41–55.

Mandal, A., Mukhopadhyay, P. & Das, S. K. 2019a The study of adsorption efficiency of rice husk ash for removal of phenol from wastewater with low initial phenol concentration. *Springer Natural Applied Sciences* **1**(2), 192–204.

Mandal, A., Mukhopadhyay, P. & Das, S. K. 2019b Efficiency analysis of rice husk as adsorbent for removal of phenol from wastewater. *Journal of Environmental and Analytical Toxicology* **9**(3), 605–612.

Mandal, A., Mukhopadhyay, P. & Das, S. K. 2020 Adsorptive removal of phenol from wastewater using guava tree bark. *Environmental Science and Pollution Research* **27**, 23937–23949. https://doi.org/10.1007/s11356-020-08777-2.

Mu'azu, N. D., Jarrah, N., Zubair, M. & Alagha, O. 2017 Removal of phenolic compounds from water using sewage sludge based activated carbon adsorption: a review. *International Journal of Environmental Research and Public Health* **14**, 1–34.

Nagda, G. K., Diwan, A. M. & Ghole, V. S. 2007 Potential of Tendu leaf refuse for phenol removal in aqueous systems. *Applied Ecology and Environmental Research* **5**(2), 1–9.

Naghipour, D., Taghavi, K., Jaafari, J., Mahdavi, Y., Ghozikali, M. G., Ameri, R., Jamshidi, A. & Mahvi, A. H. 2016 Statistical modeling and optimization of the phosphorus biosorption by modified Lemna minor from aqueous solution using response surface methodology (RSM). *Desalination and Water Treatment* **57**(41), 19431–19442.

Naghipour, D., Taghavi, K., Ashournia, M., Jaafari, J. & Movarrekh, R. A. 2018 A study of Cr(VI) and NH^{4+}adsorption using greensand (glauconite) as a low-cost adsorbent from aqueous solutions. *World and Environment Journal* **34**(1), 45–56. doi:10.1111/wej.12440.

Naiya, T. K., Bhattacharya, A. K. & Das, S. K. 2009 Clarified sludge (basic oxygen furnace sludge) - an adsorbent for removal of Pb(II)from aqueous solutions – kinetics, thermodynamics and desorption studies. *Journal of Hazardous Materials* **170**, 252–262.

Ozkaya, B. 2006 Adsorption and desorption of phenol on activated carbon and a comparison of isotherm models. *Journal of Hazardous Materials* **129**, 158–163.

Reichenberg, D. 1953 Properties of ion exchange resins in relation to their structure III kinetics of exchange. *Journal of American Chemical Society* **75**, 589–597.

Safari, G. H., Zarrabi, M., Hoseini, M., Kamani, H., Jaafari, J. & Mahvi, A. H. 2015 Trends of natural and acid-engineered pumice onto phosphorus ions in aquatic environment: adsorbent preparation, characterization, and kinetic and equilibrium modelling. *Desalination and Water Treatment* **54**(11), 3031–3043.

Sarkar, S. & Das, S. K. 2015 Removal of Cr(VI) and Cu (II) ions from aqueous solution by rice husk ash – column studies. *Desalination and Water Treatment* **57**(43), 20340–20349.

Sarkar, S. & Das, S. K. 2016 Removal of hexavalent chromium from aqueous solution using natural adsorbents – column studies. *International Journal of Engineering Research and Technology* **5**(11), 370–377.

Shokoohi, R., Movahedian, H., Dargahi, A., Jafari, A. J. & Parvaresh, A. 2017 Survey on efficiency of BF/AS integrated biological system in phenol removal of wastewater. *Desalination and Water Treatment* **82**, 315–321.

Singha, B. & Das, S. K. 2012 Removal of Pb(II) ions from aqueous solution and industrial effluent using natural biosorbents. *Environmental Science and Pollution Research* **19**(6), 2212–2226.

Singha, B. & Das, S. K. 2013 Adsorptive removal of Cu(II) from aqueous solution and industrial effluent using natural/agricultural wastes. *Colloids and Surfaces B: Biointerfaces* **107**, 97–106.

Temkin, M. J. & Pyzhev, V. 1940 Recent modifications of Langmuir isotherms. *ActaPhysicochimica, URSS* **12**, 217–222.

Tor, A., Cengeloglu, Y., Aydin, M. E. & Ersoz, M. 2006 Removal of phenol from aqueous phase by using neutralized red mud. *Journal of Colloid and Interface Science* **300**, 498–503.

Uddin, M. T., Islam, M. S. & Adedin, M. Z. 2007 Adsorption of phenol from aqueous solution by water hyacinth ash. *ARPN Journal of Engineering and Applied Sciences* **2**(2), 11–17.